# H2O2 Oxidation by Fe-III-OOH Intermediates and Its Effect on Catalytic Efficiency

Chen, Juan; Draksharapu, Apparao; Angelone, Davide; Unjaroen, Duenpen; Padamati, Sandeep K.; Hage, Ronald; Swart, Marcel; Duboc, Carole; Browne, Wesley R.

*Published in:*
ACS Catalysis

*DOI:*
10.1021/acscatal.8b02326



*Publication date:*
2018

ACS Catalysis

Research Article

Cite This: ACS Catal. 2018, 8, 9665−9674

pubs.acs.org/acscatalysis

# $H_2O_2$ Oxidation by $Fe^{III}$−OOH Intermediates and Its Effect on Catalytic Efficiency

Juan Chen,[†] Apparao Draksharapu,[†,#] Davide Angelone,[†,§] Duenpen Unjaroen,[†] Sandeep K. Padamati,[†] Ronald Hage,[‡] Marcel Swart,[§,∥] Carole Duboc,[⊥] and Wesley R. Browne*[,†]

[†]Molecular Inorganic Chemistry, Stratingh Institute for Chemistry, Faculty of Science and Engineering, University of Groningen, Nijenborgh 4, 9747AG, Groningen, The Netherlands

[‡]Catexel BV, BioPartner Center, Galileiweg 8, 2333BD Leiden, The Netherlands

[§]Institut de Química Computacional i Catàlisi (IQCC), Departament de Química, Universitat de Girona, Campus Montilivi, E17003 Girona, Catalonia, Spain

[∥]ICREA, Pg. Lluís Companys 23, 08010 Barcelona, Spain

[⊥]Departement de Chimie Moleculaire, Univ. Grenoble Alpes/CNRS, UMR-5250, BP-53, 38041 Grenoble Cedex 9, France

Supporting Information

**ABSTRACT:** The oxidation of the C−H and C=C bonds of hydrocarbons with $H_2O_2$ catalyzed by non-heme iron complexes with pentadentate ligands is widely accepted as involving a reactive $Fe^{IV}$=O species such as $[(N4Py)Fe^{IV}=O]^{2+}$ formed by homolytic cleavage of the O−O bond of an $Fe^{III}$−OOH intermediate (where N4Py is 1,1-bis(pyridin-2-yl)-*N*,*N*-bis(pyridin-2-ylmethyl)methanamine). We show here that at low $H_2O_2$ concentrations the $Fe^{IV}$=O species formed is detectable in methanol. Furthermore, we show that the decomposition of $H_2O_2$ to water and $O_2$ is an important competing pathway that limits efficiency in the terminal oxidant and indeed dominates reactivity except where only sub-/near-stoichiometric amounts of $H_2O_2$ are present. Although independently prepared $[(N4Py)Fe^{IV}=O]^{2+}$ oxidizes stoichiometric $H_2O_2$ rapidly, the rate of formation of $Fe^{IV}$=O from the $Fe^{III}$−OOH intermediate is too low to account for the rate of $H_2O_2$ decomposition observed under catalytic conditions. Indeed, with excess $H_2O_2$, disproportionation to $O_2$ and $H_2O$ is due to reaction with the $Fe^{III}$−OOH intermediate and thereby prevents formation of the $Fe^{IV}$=O species. These data rationalize that the activity of these catalysts with respect to hydrocarbon/alkene oxidation is maximized by maintaining sub-/near-stoichiometric steady-state concentrations of $H_2O_2$, which ensure that the rate of the $H_2O_2$ oxidation by the $Fe^{III}$−OOH intermediate is less than the rate of the O−O bond homolysis and the subsequent reaction of the $Fe^{IV}$=O species with a substrate.

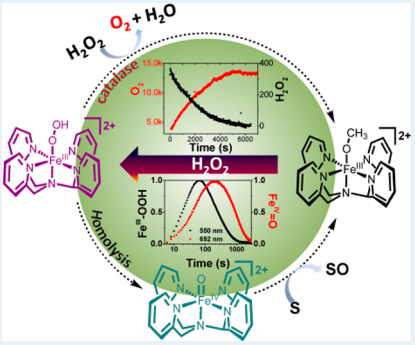


**KEYWORDS:** *iron, oxidation, peroxide, catalase, Raman spectroscopy, EPR spectroscopy*



Biomimetic analogues play a central role in understanding bioinorganic systems and enzymes, particularly in the identification of reactive intermediates and their role in catalytic processes.[1−4] In this context, high-valent iron oxo species (i.e., $Fe^{IV}$=O) have been studied intensely over the past decade,[5−9] especially since their first isolation and crystallographic characterization by Que and co-workers[10] in 2003. The synthetic non-heme $Fe^{IV}$=O complexes reported to date show a broad range of reactivity, including C−H oxidation,[7,11−14] with potencies comparable to those of non-heme and heme enzymes, such as Tau-D, and cytochrome P450.[15]

High-valent $Fe^{IV}$=O species are frequently invoked as the active species engaged in the oxidation of organic substrates by both heme and non-heme enzymes[5,7,16−18] and in biomimetic non-heme iron catalysts. The $Fe^{IV}$=O species that have been isolated to date are invaluable in determining their intrinsic reactivity, and their continuous regeneration under catalytic conditions, with $H_2O_2$ as terminal oxidant, is desirable in achieving turnover in the oxidative transformations that they engage in.

The formation of $Fe^{IV}$=O species upon homolytic O−O bond cleavage in the corresponding $Fe^{III}$−OOH complexes has been postulated to be a key step for the oxidation of organic substrates by nonheme iron catalysts with $H_2O_2$:[4,16,19] for example, in the oxidative cleavage of DNA by bleomycin−$Fe^{III}$−OOH.[20,21] Notably, in contrast to heme systems, where formation of $Fe^{V}$=O species is observed via heterolytic O−O bond cleavage (followed by oxidation of the porphyrin ligand to form compound **I**). Heterolysis of the O−O bond in low-spin non-heme iron(III)−hydroperoxy species is energetically unfavorable.[22−24]

However, to the best of our knowledge, this process ($Fe^{III}$−OOH → $Fe^{IV}$=O) was observed only recently for high-spin

Received: June 14, 2018
Revised: August 30, 2018
Published: September 6, 2018




DOI: 10.1021/acscatal.8b02326
ACS Catal. 2018, 8, 9665−9674

$Fe^{III}$−OOH species but has not yet been seen for low-spin $Fe^{III}$−OOH complexes.[25−29] Furthermore, the relatively low efficiency of non-heme iron complexes in alkane oxidations with an excess of $H_2O_2$, together with the known reactivity of $Fe^{IV}$=O species with $H_2O_2$,[30] casts doubt on the validity of this paradigm under catalytic conditions.[3]

The absence of evidence of the formation of $Fe^{IV}$=O species and loss of $H_2O_2$ through unproductive pathways (i.e., disproportionation) can be rationalized by assuming that the generated $Fe^{IV}$=O species either reacts with $H_2O_2$ or engages in, for example, C−H oxidation and hence the reaction of $Fe^{IV}$=O with $H_2O_2$ competes with its reaction with organic substrates. Indeed, Collins and co-workers have shown that the $Fe^{III}$(TAML) (TAML = tetraamidato macrocyclic ligand) system disproportionates $H_2O_2$ through a $Fe^{IV}$=O intermediate,[2] and of direct relevance to the present study, the complex $[(N4Py)Fe^{IV}{=}O]^{2+}$ (where N4Py is 1,1-bis(pyridin-2-yl)-*N*,*N*-bis(pyridin-2-ylmethyl)methanamine) was shown by Rohde and co-workers to react rapidly with $H_2O_2$ in acetonitrile.[30]

In the case of complexes based on pentadentate ligands, e.g., N4Py (Figure 1), the apparent stability of the $Fe^{III}$−OOH intermediate and absence of direct spectroscopic evidence for the formation of $Fe^{IV}$=O from it make it challenging to identify the actual mechanisms involved in substrate oxidation and $H_2O_2$ disproportionation.

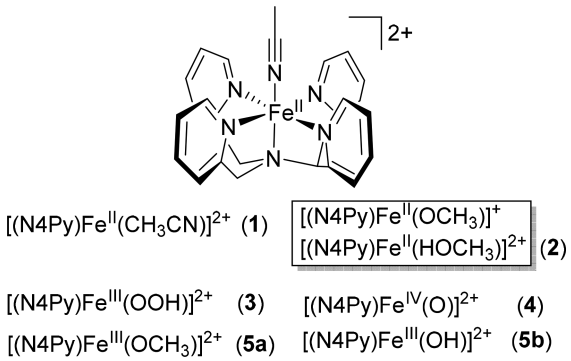


**Figure 1.** Structures of the complexes and intermediates discussed in the present study.

Here, using a combination of time-resolved UV−vis absorption, (resonance) Raman, and EPR spectroscopy and computational chemistry, we demonstrate that, contrary to expectations, the rate of O−O bond homolysis in $[(N4Py)Fe^{III}$−$OOH]^{2+}$ to form $[(N4Py)Fe^{IV}{=}O]^{2+}$ and a hydroxyl radical is much lower than the rate of $H_2O_2$ disproportionation observed under reaction conditions. We show that the $Fe^{III}$−OOH species is responsible for $H_2O_2$ decomposition. As a result, the efficiency of substrate oxidation is negatively affected by an increase in the steady-state $H_2O_2$ concentration, since formation of $Fe^{IV}$=O species is uncompetitive.

## EXPERIMENTAL DETAILS

**Synthesis.** The ligand 1,1-bis(pyridin-2-yl)-*N*,*N*-bis(pyridin-2-ylmethyl)methanamine (N4Py),[31] $[(N4Py)Fe^{II}(CH_3CN)](ClO_4)_2$ (**1**),[21,31,32] and $[(N4Py)Fe^{IV}{=}O](PF_6)_2$ (**4**)[33] were prepared as reported previously. Commercially available chemicals were purchased from Sigma-Aldrich without further purification. All solvents used for spectroscopy were of UVASOL (Merck) grade. $H_2O_2$ was 50 wt % in $H_2O$ from Sigma-Aldrich and was diluted in methanol as required. The concentration of $H_2O_2$ in methanol was confirmed by Raman spectroscopy (see Figure S7 for details).

**Physical Methods.** UV−vis absorption spectra were recorded with a Specord600 (Analytik Jena) spectrophotometer in 1 cm (unless stated otherwise) path length quartz cuvettes. Raman spectra at $\lambda_{exc}$ 785 nm were recorded on a PerkinElmer Raman Station at room temperature. Raman spectra at 355 nm (10 mW at source, Cobolt Lasers) were acquired in a 180° backscattering arrangement. Raman scattering was collected by a 2.5 cm diameter plano convex lens ($f$ = 7.5 cm). The collimated Raman scattering passed through an appropriate long pass edge filter (Semrock) and was focused by a second 2.5 cm diameter plano convex lens ($f$ = 15 cm) into a Shamrock500i spectrograph (Andor Technology) 2399 L/mm grating blazed at 300 nm, acquired with an iDus-420-BU2 CCD camera (Andor Technology). The spectral slit width was set to 12 $\mu$m. Data were recorded and processed using Solis (Andor Technology) with spectral calibration performed using the Raman spectrum of acetonitrile/toluene, 50/50 (v/v).[34] EPR spectra (X-band, 9.46 GHz) were recorded on a Bruker ECS106 spectrometer in liquid nitrogen (77 K) or a Bruker EMX Nano spectrometer. Samples for measurements were transferred to a quartz 3 mm EPR tube (0.5 mL) and flash frozen in liquid nitrogen immediately, concurrent with monitoring by UV−vis absorption spectroscopy.

**Computational Details.** Computational studies were performed using ADF and QUILD,[35−37] as reported earlier.[38] Briefly, geometry optimization and frequency calculations were performed using the unrestricted density functional BP86-$D_3$[39−41] with a triple-$\zeta$ valence plus polarization basis set on iron combined with a double-$\zeta$ valence plus polarization on all other atoms (TDZP). Single-point energy calculations on these geometries were made with the S12g spin-state consistent functional[42,43] in a triple-$\zeta$ valence plus double polarization (TZ2P) basis set. Free energy ($\Delta G$) corrections were obtained from the BP86-$D_3$ data and are corrected for zero point energy (ZPE); thermal and entropic corrections were made from frequency calculations at 298 K. The solvation energy was considered using methanol as a solvent with the COSMO solvation model as implemented in ADF.[44]

*Caution!* The drying or concentration of solutions that potentially contain $H_2O_2$ should be avoided. Prior to drying or concentrating, the presence of $H_2O_2$ should be tested for using peroxide test strips followed by neutralization on solid $NaHSO_3$ or another suitable reducing agent. In work with $H_2O_2$, suitable protective safeguards should be in place at all times due to the risk of explosion. In experiments where complex **2** is mentioned, it was prepared by dissolution of **1** in methanol (Figure S1).

*Caution!* In work with perchlorate salts, suitable protective safeguards should be in place at all times due to the risk of explosion. Perchlorate salts should be handled in small (milligram) quantities and used only where necessary.

## RESULTS AND DISCUSSION

Typically, acetonitrile is the solvent of choice for the reaction of non-heme iron complexes with oxidants such as $H_2O_2$.[45] However, in acetonitrile, the formation of $[(N4Py)Fe^{III}$−$OOH]^{2+}$ (**3**) is observed only with a large excess (>50 equiv) of $H_2O_2$ and the subsequent formation of $[(N4Py)Fe^{IV}{=}O]^{2+}$ (**4**) has not been observed,[21] despite the fact that **4**, prepared independently, is itself stable in acetonitrile even at room temperature. This is in part due to the stability ($E_{1/2}$ = 1.2 V vs



DOI: 10.1021/acscatal.8b02326
ACS Catal. 2018, 8, 9665−9674

SCE) of $[(N4Py)Fe^{II}–NCCH_3]^{2+}$ (**1**) toward electron transfer oxidation and in part due to the high binding constant of the $CH_3CN$ ligand in comparison with water or $H_2O_2$. In the present study methanol was chosen to circumvent the formation of such kinetically inert $CH_3CN$ complexes. In methanol, the $CH_3CN$ ligand of **1** exchanges immediately, to form **2** (which is either $[(N4Py)Fe^{II}–OCH_3]^{+}$or $[(N4Py)Fe^{II}–HOCH_3]^{2+}$ see the Supporting Information for a discussion), as manifested in a decrease and red shift in the near-UV and visible absorption bands (Figure S1).[32] The exchange of the methanol/methoxido ligand for water and $H_2O_2$ is relatively rapid in both the ferrous and ferric states (vide infra), which is central to enabling observation of other species involved in the reactions discussed and is in stark contrast to the slow ligand exchange seen for **1** in acetonitrile.

**Reaction of 2 with Near-Stoichiometric $H_2O_2$ and Homolysis of O–O Bond of $[(N4Py)Fe^{III}\text{-}OOH]^{2+}$.** Addition of 0.6 equiv of $H_2O_2$ to **2** results in immediate (<2 s) conversion to $[(N4Py)Fe^{III}–OCH_3)]^{2+}$ (**5a**) with its characteristic X-band EPR spectrum at $g$ = 2.29, 2.12, and 1.96.[46] With 1.2 equiv of $H_2O_2$, $[(N4Py)Fe^{III}–OOH]^{2+}$ (**3**) is obtained in minor amounts by both UV–vis absorption and EPR spectroscopy ($g$ = 2.16, 2.11, and 1.98;[21] Figure S2). Addition of 2 equiv of $H_2O_2$ to **2** results in the formation of $[(N4Py)Fe^{III}–OOH]^{2+}$ (**3**) (Figure 2) by ligand exchange over 50 s at room

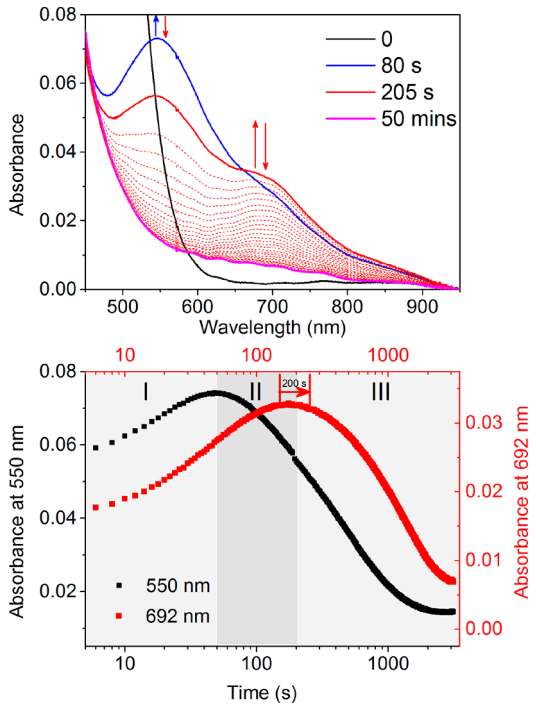


**Figure 2.** (top) UV–vis absorption spectrum of **2** (0.25 mM) in methanol before (black) and after addition of 2 equiv of $H_2O_2$ at 21 °C. (bottom) Corresponding change in absorbance over time at 550 and 692 nm. Path length: 2 cm.

temperature, reaching a maximum of 14% (based on the absorbance at 550 nm, Figure 2-I) before decreasing again over 1000 s. The decrease in absorbance at 550 nm (of **3**) proceeds concomitant with an increase in absorbance at 692 nm due to $Fe^{IV}$=O (**4**, Figure 2-II/III). Since **4** reacts rapidly (200 s) with even stoichiometric $H_2O_2$ (vide infra), its appearance indicates that the concentration of $H_2O_2$ in solution is already negligible by 80 s (vide infra). The absorbance at 692 nm remains almost constant over 200 s during the decay of **3**. The hydroxyl radical formed due to O–O bond homolysis will react with methanol ($9.7 \times 10^{-8}$ $s^{-1}$) to form a methoxy radical that can react with $H_2O_2$ or other species to yield either methanol or formaldehyde.

Once **3** has been fully consumed, the absorbance at 692 nm then decreases concomitant with the formation of more $[(N4Py)Fe^{III}–OCH_3]^{2+}$ (**5a**). These data are consistent with a prior equilibrium between **5a** and **3** followed by O–O bond homolysis to form **4**. Once sufficient $H_2O_2$ is consumed, the concentration of **4** is dependent only on the rate of its formation from **3** and the rate of its loss by reaction with methanol (vide infra). The rate of formation of **4** through homolysis of the O–O bond of $[(N4Py)Fe^{III}–OOH]^{2+}$ (**3**) under these conditions is low (<$2.2 \times 10^{-4}$ $s^{-1}$, vide infra), which is consistent with the reaction's endergonicity; calculated (see the Supporting Information) at 19.1 kcal $mol^{-1}$. The value is also consistent with the reported value calculated for the related homolytic cleavage in activated Fe–bleomycin.[18,23]

$$[(N4Py)Fe^{III}(OOH)]^{2+} \rightarrow [(N4Py)Fe^{IV}(O)]^{2+} + \dot{O}H$$
$$\Delta G = 19.1 \text{ kcal mol}^{-1} \quad (1)$$

**Disproportionation of $H_2O_2$ by 3 in Methanol.** Addition of excess $H_2O_2$ (>40 equiv) to **2** in methanol results in immediate oxidation to **5a** (i.e., a complete loss in absorbance at 450 nm within the mixing time, 2 s; Figure S3). The oxidation is followed by full conversion of **5a** to $[(N4Py)Fe^{III}–OOH)]^{2+}$ (**3**) over 5–10 s. The $H_2O_2$ concentration was monitored in real time by Raman spectroscopy. The second-order rate constant for the formation of **3** from **5a**, determined under pseudo-first-order conditions (2.5–50 mM $H_2O_2$, Figure 3 and Figure S4), is 10.5(±0.1) $M^{-1}$ $s^{-1}$ at 21 °C, consistent with the exothermicity (−10.2 kcal $mol^{-1}$) and low barrier for the exchange of the sixth ligand.

$$[(N4Py)Fe^{III}(OCH_3)]^{2+} + H_2O_2 \rightarrow [(N4Py)Fe^{III}(OOH)]^{2+} + CH_3OH$$
$$\Delta G = -10.2 \text{ kcal mol}^{-1} \quad (2)$$

EPR spectra of samples flash frozen to 77 K (Figure S5) immediately after addition of an excess of $H_2O_2$ show two well-resolved $S$ = 1/2 signals, characteristic of **3** (major species) and **5a** (minor species). Samples, flash frozen after 18 min, show that the signals of **3** are diminished with the concomitant increase of in the signals of **5a**, and at ca. 50 min, the signals of **3** are absent, leaving only a more intense signal from **5a**.

Notably, both the maximum extent of formation of **3** and the time between addition of $H_2O_2$ and the start of the subsequent decrease in the absorbance of **3** are dependent on the initial concentration of $H_2O_2$ (Figure 3). These data indicate that $H_2O_2$ consumption is relatively similar to the rate of formation of **3** from **5a**. The rate of decrease of the absorbance due to **3** is independent of the initial $H_2O_2$ concentration (Figure S6), because the decay occurs only after essentially all of the $H_2O_2$ has been consumed, as confirmed by Raman spectroscopy ($\lambda_{exc}$ 785 nm, Figure 4). Time-resolved Raman spectroscopy shows that the concentration of $H_2O_2$ decreases from $t$ = 0 while the resonantly enhanced bands of **3** ($Fe^{III}–OOH$) at 632, 650, 670, and 798 $cm^{-1}$ do not decrease in intensity until the signal ($\nu$(O–O)) from $H_2O_2$ at 872 $cm^{-1}$ has decreased to near-stoichiometric levels at least (i.e., below the limit of detection of ca. 10 mM, Figure S7).



DOI: 10.1021/acscatal.8b02326
ACS Catal. 2018, 8, 9665–9674

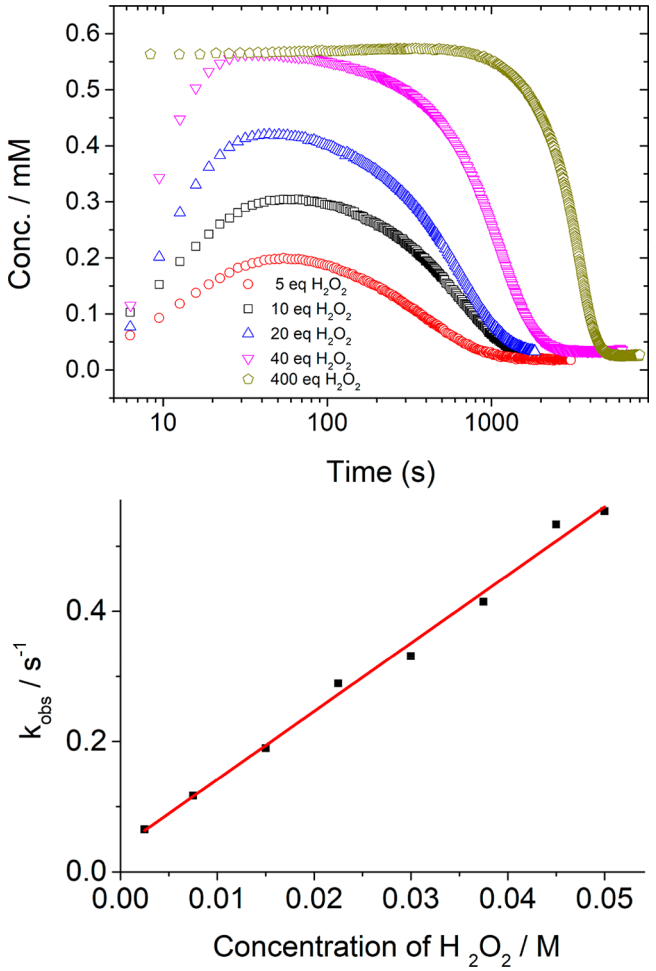


**Figure 3.** (top) Concentration of $[(N4Py)Fe^{III}–OOH]^{2+}$ (**3**, from absorbance at 550 nm) against log(time) for various amounts of $H_2O_2$ added (5 (red), 10 (black), 20 (blue), 40 (pink), and 400 (khaki) equiv) to **1** (0.56 mM) at 21 °C in methanol. (bottom) Pseudo-first-order rate constant $k_{obs}$ for the formation of $[(N4Py)Fe^{III}–OOH)]^{2+}$ vs concentration of $H_2O_2$.

**Regeneration of $Fe^{III}$–OOH and $O_2$ Evolution.** For the absorption at 550 nm and its EPR signals, the characteristic Raman bands of **3** appear within the time resolution of the measurement (<60 s) upon addition of excess $H_2O_2$ and maintain their intensity until all $H_2O_2$ has been consumed. These data are consistent with the continuous regeneration of **3** from $[(N4Py)Fe^{III}–OR)]^{2+}$ (where R = H, $CH_3$) and $H_2O_2$. **3** is the resting state in the cycle, and the formation of **3** from **5a** is a rapid equilibrium prior to the rate-determining step in the reaction.

Headspace analysis by Raman spectroscopy (Figure 5 and Figure S8) confirms generation of $O_2$ at a rate corresponding to the rate of decrease of $H_2O_2$. Details for the quantification of $O_2$ generated are provided in section 3 of the Supporting Information.

The relation between the rate of consumption of $H_2O_2$ and concentration of **3** is apparent when $H_2O_2$ is present in excess (>50 equiv). The concentration of **3** remains constant (>80% of total iron concentration) for a period of time, the duration of which is dependent on the initial concentration of **2** (Figure S8). The concentration of $H_2O_2$, determined by Raman spectroscopy, during this period shows an exponential decay (Figure 6 and Figure S9). The observed rate constant ($k_{obs}$) for

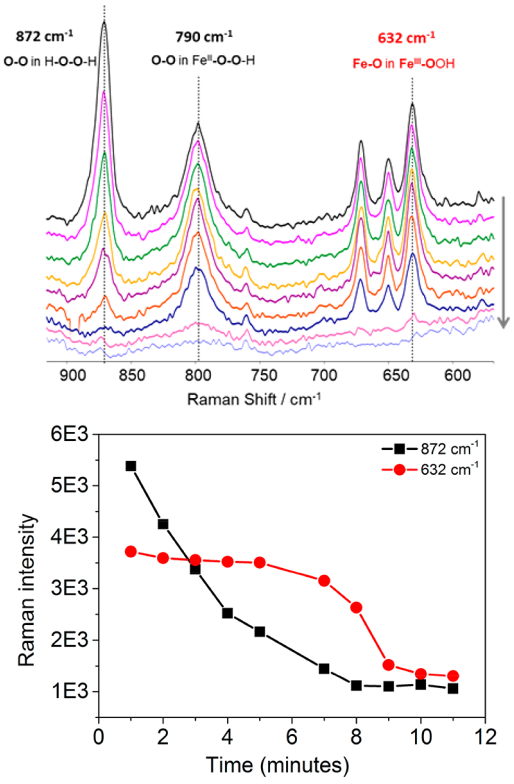


**Figure 4.** (top) Raman spectra of **1** (ca. 5 mM) in methanol over time after addition of 50 equiv of $H_2O_2$ at $\lambda_{exc}$ 785 nm. (bottom) Change in intensity of Raman bands at 872 (of $H_2O_2$) and 632 $cm^{-1}$ (of **3**) over time at 21 °C. Spectra correspond to the data points shown.

the decomposition of $H_2O_2$ is linearly dependent on the catalyst concentration (i.e., [**3**], Figure 6), with a second-order rate constant of 0.8 $M^{-1}$ $s^{-1}$ at 21 °C (Figure S9). The rate constant is less than that for the formation of **3** (10.5(±0.1) $M^{-1}$ $s^{-1}$) and is thus in agreement with **3** as the resting state in the catalytic cycle under steady-state conditions.

**Reaction of $[(N4Py)Fe^{IV}{=}O]^{2+}$ (4) with Methanol and $H_2O_2$.** The self-decay rate of **4** (prepared independently),[33] due to reaction with solvent, is low in acetonitrile[30] but is significant in methanol (Figure 7). In methanol, the NIR absorbance of **4** decays exponentially over 1000 s with the concomitant production of 1 equiv of **5a** ($Fe^{III}–OCH_3$) and 0.5 equiv of formaldehyde (see the Supporting Information for details). The kinetic isotope effect for this decay in $CD_3OD$ is ca. 10 (Figure 7).[33] OH/OD exchange does not affect this rate, which is consistent with the competence of **4** in the oxidation of methanol with a rate-determining hydrogen atom abstraction (HAT) step at the C–H bond.

Addition of 1 equiv of $H_2O_2$ to **4** ($Fe^{IV}{=}O$) in methanol results in conversion to **5a** ($Fe^{III}–OCH_3$) within 200 s, in agreement with data reported in acetonitrile (second-order rate constant of 8 $M^{-1}$ $s^{-1}$ at 21 °C),[30] and is ca. 10 times faster than the reaction of **4** with $CH_3OH$. However, in stark contrast with the 2:1 ratio of **4** to $H_2O_2$ required in acetonitrile[30] for full reduction of **4** to the $Fe^{III}$ state, in methanol only 1 equiv of $H_2O_2$ is required (Figure S10). In both solvents the need for excess $H_2O_2$ (>0.5 equiv) indicates that $H_2O_2$ is consumed by other pathways.

$$2[(N4Py)Fe^{IV}(O)]^{2+} + H_2O_2 \rightarrow 2[(N4Py)Fe^{III}(OH)]^{2+} + O_2 \quad (3)$$



DOI: 10.1021/acscatal.8b02326
ACS Catal. 2018, 8, 9665–9674

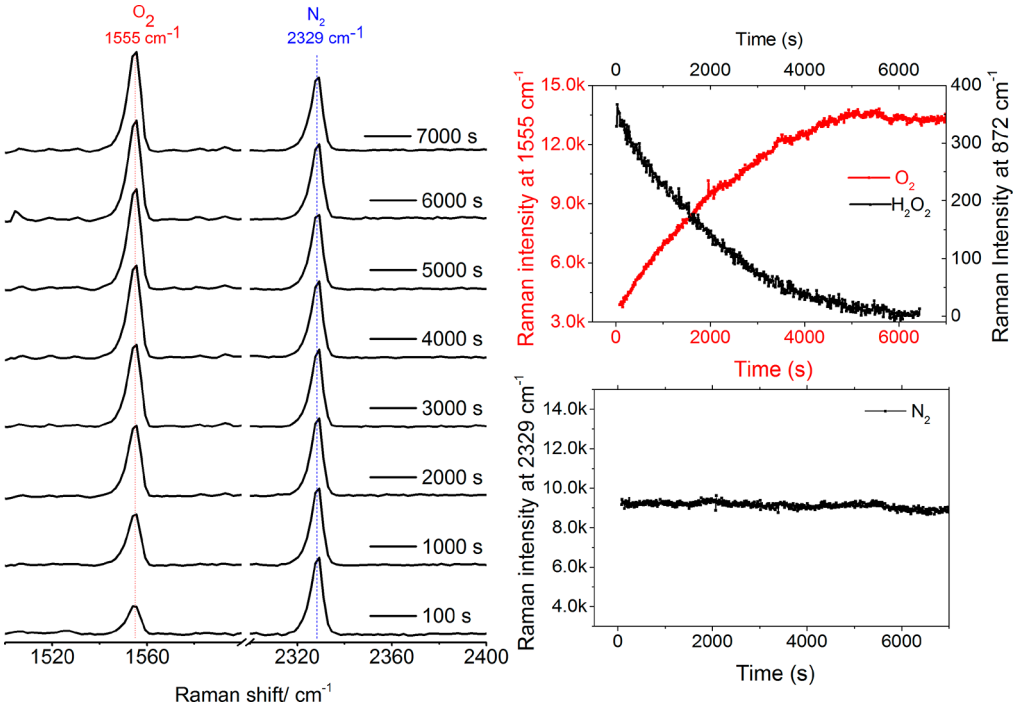


**Figure 5.** (left) Raman spectra ($\lambda_{exc}$ 532 nm) obtained from the headspace above the reaction mixture containing **1** (0.25 mM) and 200 mM $H_2O_2$ in methanol at 21 °C. (right) Change in intensity of Raman band at 1555 $cm^{-1}$ of $O_2$ (head space, red, $\lambda_{exc}$ 532 nm, internal reference was 2329 $cm^{-1}$ band of $N_2$) and at 872 $cm^{-1}$ for $H_2O_2$ (liquid phase, black, $\lambda_{exc}$ 785 nm).

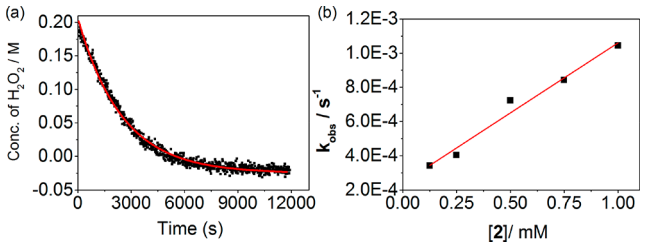


**Figure 6.** (a) Concentration of $H_2O_2$ with time following addition of $H_2O_2$ (200 mM) to **2** (0.25 mM) at 21 °C. (b) Plot of the pseudo-first-order rate $k_{obs}$ versus concentration of **2**.

The OH/D kinetic isotope effect observed in the reduction of **4** with $H_2O_2$ is masked to some extent by the competing reaction of **4** with $CH_3OD$ (vide supra) but is nevertheless consistent with an HAT mechanism.

In contrast to $CH_3OH$, in $CD_3OD$ the decay of **4** upon addition of 1 equiv of $D_2O_2$ is biphasic. Deuterium atom abstraction (from C−D in $CD_3OD$) by **4** is much slower than the reaction of **4** with 1 equiv of $D_2O_2$. Consequently, the initial rate (i.e., within 10 min after addition of $D_2O_2$, 1.13 × $10^{-3}$ $s^{-1}$) of decay in the absorbance of **4** is due to reaction with the peroxide only. After this period the rate of decay decreases (to 9.5 × $10^{-5}$ $s^{-1}$), which corresponds to the decay of **4** in $CD_3OD$ alone (Figure 7b). A biphasic decay is observed in $CH_3OD$ also but is much less pronounced due to the relatively rapid rate of reaction of **4** with $CH_3OD$ also.

These data indicate that, in addition to reaction with **4**, $D_2O_2$ is consumed through a second pathway, i.e. by the $Fe^{III}$ species formed initially, which is only apparent when the background reaction of **4** with solvent is slow (i.e., in the case of $CD_3OD$). The decreased extent of reduction of **4** with 1 equiv of $D_2O_2$ is similar to that observed in acetonitrile earlier.[30] Although calculation of the KIE for reaction of **4** with $H_2O_2/D_2O_2$ is estimated as close to 10, indicating that HAT is likely to be rate limiting, the occurrence of several reactions in parallel precludes mechanistic interpretation of this value.

With excess $H_2O_2$ (40 equiv) in $CH_3OH$, the characteristic NIR absorbance of **4** disappears over 10 s, while that of **3** ($Fe^{III}$−OOH, Figure S11) appears concomitantly. These data indicate that the reduction of **4** to **5a** by $H_2O_2$ is followed by ligand exchange with $H_2O_2$ to form **3**. Thereafter, the spectral changes are essentially the same as those observed upon addition of $H_2O_2$ to **2** in methanol.

In summary, the rate of reaction of **4** follows the order $H_2O_2$ (in $CH_3OH$) > $D_2O_2$ (in $CH_3OD$) > $D_2O_2$ (in $CD_3OD$). Notably, the presence of even 1 equiv of $H_2O_2$ precludes the presence of **4** in methanol, rationalizing the fact that **4** can be observed only when the concentration of $H_2O_2$ is substoichiometric. The rate of reduction of **4** by $H_2O_2$ in acetonitrile was reported by Braymer et al.[30] to be insensitive to deuteration (i.e., $D_2O_2$). In retrospect this observation can be understood by considering the need for an excess of $H_2O_2$ in that case and the fact that **4** is not the sole species capable of reacting with $H_2O_2$.

**Mechanistic Considerations.** The paradigm for oxidation catalysis with complexes such as **2** and $H_2O_2$ is rapid oxidation to the ferric state and formation of hydroperoxido complexes (e.g., $[(N4Py)Fe^{III}-OOH)]^{2+}$, **3**). Homolytic cleavage of the O−O bond in **3** yields $[(N4Py)Fe^{IV}=O]^{2+}$ (**4**) and a hydroxyl radical, both of which are responsible for oxidation of organic substrates. In the present case, only **3**, and not **4**, is observed in the presence of excess $H_2O_2$ (Figures 2 and 3), which is consistent with the homolytic cleavage of the O−O bond in **3** being rate determining.

The efficiency in the oxidation of organic substrates is diminished substantially in the presence of excess $H_2O_2$ due to disproportionation to $H_2O$ and $O_2$. In the present study, independently prepared **4** is shown to be reduced to the ferric



DOI: 10.1021/acscatal.8b02326
ACS Catal. 2018, 8, 9665−9674

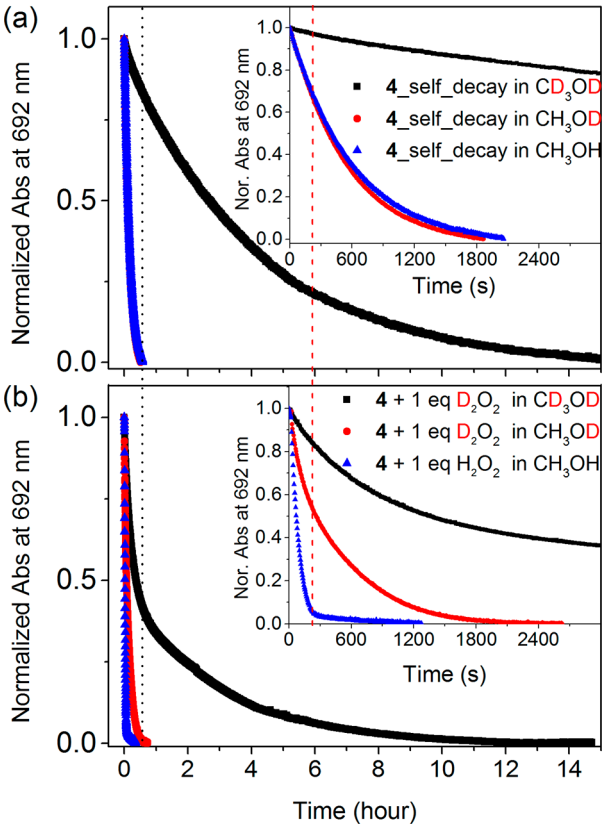


**Figure 7.** Normalized absorbance of **4** (1 mM) at 692 nm in $CH_3OH$ (blue), $CH_3OD$ (red), and $CD_3OD$ (black) with time in the (a) absence and (b) presence of 1 equiv of $D_2O_2$. Corresponding UV−vis spectra are shown in Figure S10.

state in methanol rapidly upon addition of $H_2O_2$. Hence, the fact that **4** is not observed in the presence of excess $H_2O_2$ can be ascribed to this reaction pathway (b in Scheme 1). Indeed,

**Scheme 1. Possible Mechanisms for Reaction of 2 with Excess $H_2O_2$**

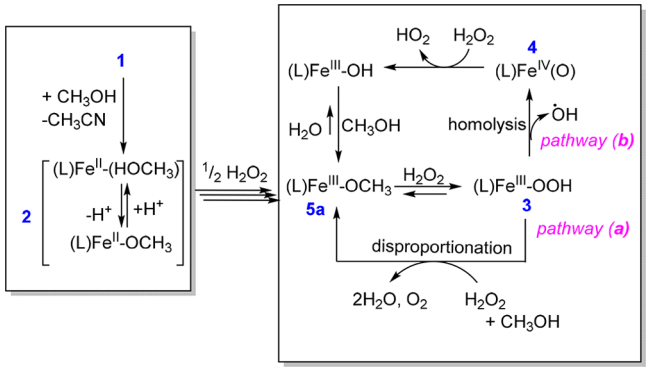


$[(N4Py)Fe^{IV}{=}O]^{2+}$ (**4**) reacts with $H_2O_2$ ($k$ = 8 $M^{-1}$ $s^{-1}$) much more rapidly than the observed rate of decomposition of $H_2O_2$ ($k$ = 0.8 $M^{-1}$ $s^{-1}$). However, pathway b (Scheme 1) will be kinetically possible only if the rate of the O−O bond homolysis of **3** is sufficiently rapid to account for the rate of decomposition of $H_2O_2$.

In the present study several observations cast doubt on the validity of pathway b. In methanol, the formation of **4** from **3** is observed once (nearly) all $H_2O_2$ has been consumed; however, the rate of this reaction is much lower (<3.0 × $10^{-3}$ $s^{-1}$, Figure 2) than expected. DFT calculations (vide infra) indicate that the cleavage of the O−O bond is substantially uphill and is accompanied by a low barrier to return to **3** (and hence has an intrinsically substantial thermal barrier). Consequently, the rate of formation of $[(N4Py)Fe^{IV}{=}O]^{2+}$ (**4**) is insufficient to account for the decomposition of $H_2O_2$ when $H_2O_2$ is present in excess. This conclusion holds the further consequence that the formation of **4** and hence the oxidation of organic substrates by **4** is not competitive with oxidation of $H_2O_2$ by **3** (pathway a, Scheme 1). The consequence of this is that the oxidation of organic substrates is only competitive under conditions of low $H_2O_2$ concentration.

**DFT Calculations.** The mechanism and comparison of two possible pathways for the reaction of **3** with $H_2O_2$ were explored through DFT calculations. Geometry optimization and frequency calculations were carried out at the BP86-$D_3$/TDZP level, with subsequent single point energies at the S12g/TZ2P level, including COSMO-ZORA self-consistently at all stages. All data are given in the Supporting Information.

The doublet ground state calculated for **3** is in accordance with experiment. However, for consistency, the reaction pathways a and b (Scheme 1) were calculated in all three possible spin states: doublet, quartet, and sextet (Figure S12). For both pathways the reaction barriers are much lower in the low-spin state in comparison to those in the other two spin states, and hence the discussion below considers only the low-spin states (Figures 8 and 9).

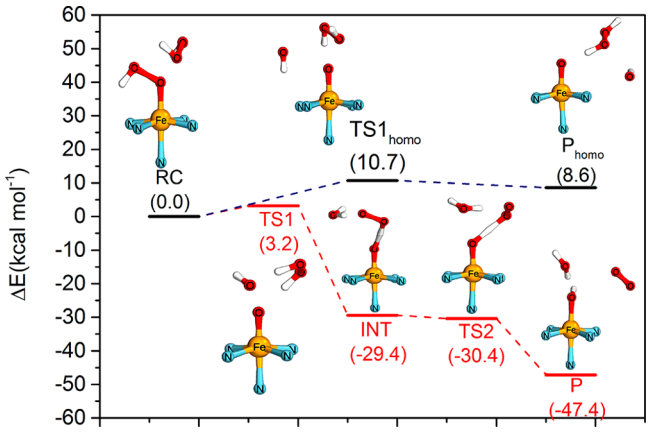


**Figure 8.** Comparison of energy profiles (in kcal $mol^{-1}$) of pathway a (catalase, in red) and pathway b (homolysis, in black), as obtained at the S12g/TZ2P//BP86-$D_3$/TDZP level. (The complete structures indicated in the profile can be also found in Figure 9.)

For the disproportionation pathway a, the reactants, **3** + $H_2O_2$, initially form a reactant complex (RC) where the peroxide is bound to the iron complex weakly. This step is followed (in TS1) by hydrogen atom abstraction from the peroxide toward the distal OH group of **3**, and simultaneously cleavage of the O−O bond of **3** takes place with a barrier of only 3.2 kcal $mol^{-1}$. In this TS, the O−O bond in **3** elongates from 1.60 to 2.14 Å, together with a shortening of the H−(OH) distance to 1.45 Å. This is followed by a highly exergonic (−32.6 kcal $mol^{-1}$) completion of the hydrogen atom transfer process to form $H_2O$ in the intermediate (INT). Simultaneously, the O−O bond of the peroxide shortens from 1.49 to1.35 Å. Formation to the product from INT involves a second hydrogen atom abstraction (barrierless in terms of Gibbs free energy (−1.0 kcal $mol^{-1}$)


DOI: 10.1021/acscatal.8b02326
ACS Catal. 2018, 8, 9665−9674

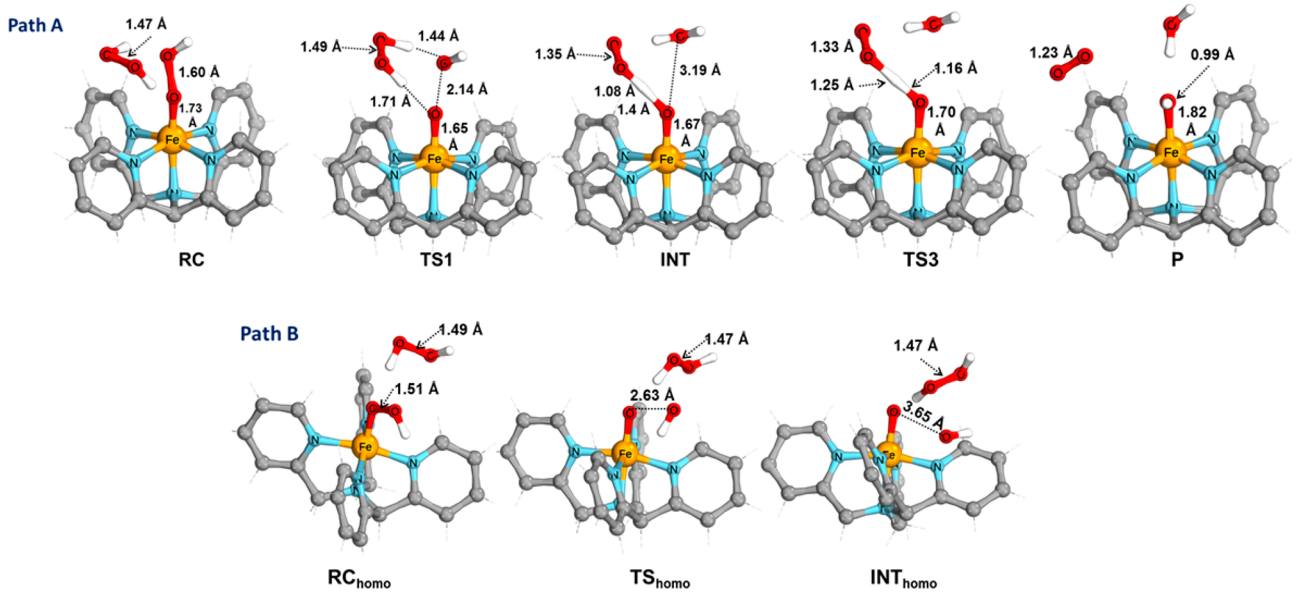


**Figure 9.** Geometries (bond distance in Å) for key species for both path A (catalase) and path B (homolysis).

and electronic energy (+1.1 kcal mol$^{-1}$)) in which the remaining hydrogen of the peroxide is transferred to the oxygen coordinated to iron. This second HAT is exergonic by ca. −17.0 kcal mol$^{-1}$ and finally leads to the products Fe$^{III}$−OH + $H_2O$ + $O_2$.

In contrast, the homolysis pathway b initially forms a similar weakly bound complex in the RC$_{homo}$. However, the activation barrier (10.7 kcal mol$^{-1}$) for homolytic cleaving of the O−O bond of **3** in TS$_{homo}$ alone to form Fe$^{IV}$=O is much higher than that in pathway a. The O−O bond in **3** elongates from 1.51 to 2.63 Å with hardly any change in the structure of the peroxide: i.e., the peroxide does not participate actively in the reaction but merely acts as a hydrogen-bond donor. More importantly, the product for this homolytic pathway b, P$_{homo}$, is so close in energy to the TS$_{homo}$ (<2 kcal mol$^{-1}$) that it readily undergoes the reverse reaction to the initial reactants.

These data are consistent with the observed low rate at which **4** forms from **3** and the rapid consumption of $H_2O_2$ by direct reaction of **3** with hydrogen peroxide in the disproportionation pathway a.

In summary, there are two pathways that should be considered for the decay of **3**. The first is a unimolecular homolysis to form **4** (Fe$^{IV}$=O) and a hydroxyl radical. This process is slow and only occurs when the concentration of $H_2O_2$ is sufficiently low such that it is outside of the solvation sphere of **3**. In this case, both **4** (Fe$^{IV}$=O) and HO$^{\bullet}$ are eventually formed and are responsible for the oxidation of organic substrates (i.e., methanol), and hence it is a productive reaction.

At higher concentrations of $H_2O_2$, i.e. where $H_2O_2$ is likely to be within the solvation sphere of **3**, the formation of two H bonds supports the breaking of the O−O bond of **3**, and either (Scheme 2) (i) stabilizes the formation of **4** ("insertion" of $H_2O_2$ into the O−O bond of **3**) or (ii) undergoes HAT to form water and HOO$^{\bullet}$ from $H_2O_2$ and, in a subsequent step, a second HAT from HOO$^{\bullet}$ by Fe$^{IV}$=O to form [(L)Fe$^{III}$(OH)]$^{2+}$ (**5b**) and dioxygen.

Our computational data show that the barrier (Scheme 2) to pathway i is substantial and endergonic (10.7 kcal mol$^{-1}$), even with stabilization through H bonding with $H_2O_2$. The barrier to pathway ii is much lower (ca. 3.2 kcal mol$^{-1}$), and leads to

**Scheme 2. Homolysis of the O−O Bond in 3 To Form 4 vs Reaction of 3 with $H_2O_2$**

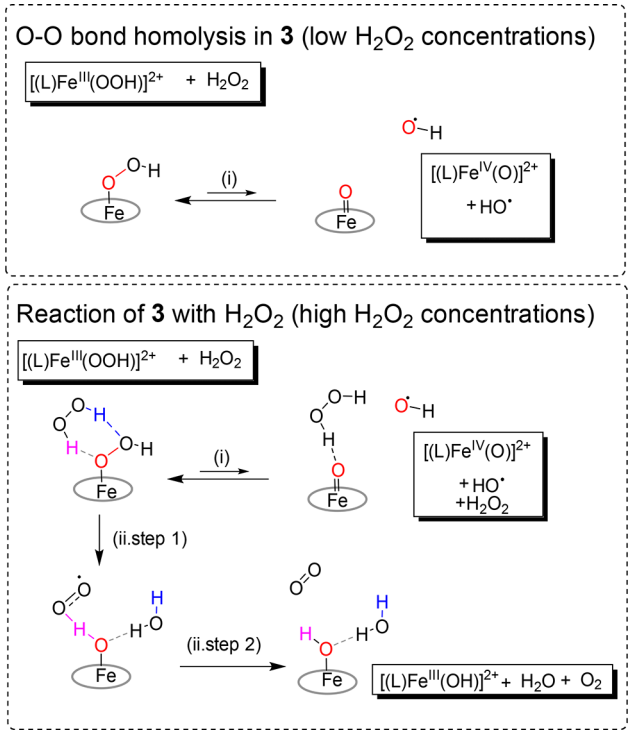


the generation of dioxygen (observed experimentally). Hence, in the presence of $H_2O_2$, **3** is almost exclusively transformed into **5b**, with subsequent solvent exchange to **5a** (and subsequently through the exchange of methoxido by another $H_2O_2$ back to **3**). Therefore, in the presence of excess $H_2O_2$, disproportionation into $H_2O$ and $O_2$ is the more energetically favored pathway.

Regardless of the pathway, the observed reactivity presents a dichotomy toward the use of complexes such as **2** for oxidation catalysis. **3** (Fe$^{III}$−OOH) does not appear to react directly with organic substrates (Figure S13),[47] and hence formation of **4** (Fe$^{IV}$=O) and a hydroxyl radical from **3** through O−O bond



DOI: 10.1021/acscatal.8b02326
ACS Catal. 2018, 8, 9665−9674

homolysis is required. However, both **3** ($Fe^{III}$–OOH) and **4** ($Fe^{IV}$=O) react with $H_2O_2$ more readily than with methanol. Therefore, ideally the steady-state concentration of $H_2O_2$ should be held as low as possible, yet still sufficiently high to generate **3** and subsequently **4** ($Fe^{IV}$=O)/HO•. Hence, the rate of addition of $H_2O_2$ should affect the relative efficiency of **2** in the oxidation of organic substrates, as shown below for the oxidation of methanol.

**Competition between the Oxidation of Methanol and $H_2O_2$ Disproportionation Catalyzed by 2.** The oxidation of methanol to methanal occurs concomitantly with the conversion of **4** ($Fe^{IV}$=O) to $[(N4Py)Fe^{II}–OCH_3)]^+$ (vide supra). However, the rate of this reaction is sufficiently low to exclude it as being an important pathway for **2** in the presence of excess $H_2O_2$ (i.e., both $Fe^{III}$–OOH and **4** ($Fe^{IV}$=O) react much more rapidly with $H_2O_2$ than with methanol). A number of competing kinetically competent pathways are thus available in the reaction of **2** with $H_2O_2$, and variation in the steady-state concentrations of reaction components should indicate the relative importance of each of these pathways.

With an 800-fold excess of $H_2O_2$, ca. 27% of $H_2O_2$ is disproportionated to $H_2O$ and $O_2$ (see the Supporting Information for a detailed $O_2$ concentration calculation), with only 2% generating formaldehyde (Figure 10, bar on the far left). Addition of

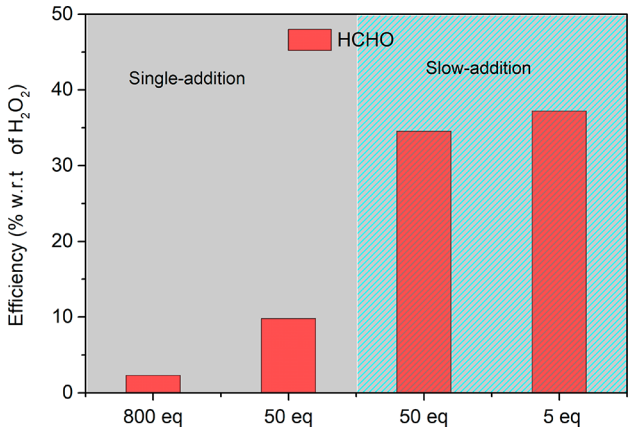


**Figure 10.** Oxidation of methanol (solvent) with $H_2O_2$ catalyzed by **1** (0.25 mM). HCHO was quantified colorimetrically (see the Supporting Information for details). The number of equivalents of $H_2O_2$ is with respect to **2**. *Slow addition* of $H_2O_2$ indicates a rate of addition of 0.4 equiv $min^{-1}$ (the two rightmost bars).

fewer equivalents of $H_2O_2$ (second bar from the left) results in a substantial increase in the efficiency in the use of $H_2O_2$ to oxidize methanol, which increases further by addition of the same amount of $H_2O_2$ slowly (Figure 10, the two rightmost bars). Adding fewer equivalents slowly over the same time does not increase efficiency further, nor does a change in the concentration of the catalyst (0.25 vs 0.125 mM), since overall conversion rates are controlled by the rate of addition. These data are consistent with the self-decay rate of **4** ($Fe^{IV}$=O) (vide supra), setting the upper limit for the rate of addition of oxidant to achieve maximum efficiency.

## CONCLUSIONS

The species accepted, i.e. $Fe^{IV}$=O, to be responsible for the oxidation of organic substrates by most non-heme iron catalysts is formed from an $Fe^{III}$–OOH precursor through O–O bond homolysis, liberating a hydroxyl radical concomitantly. Roelfes and co-workers[3] have noted that, in systems where low-spin $Fe^{III}$–OOH species are generated (with excess $H_2O_2$) and observed, the corresponding $Fe^{IV}$=O species is not observed.

Here we show that, in the case of non-heme N5 coordinated iron complexes that form observable $Fe^{III}$–OOH species, two key reasons can be invoked to rationalize the absence of a corresponding $Fe^{IV}$=O species. The first is that, even if it does form, it reacts rapidly and unproductively with $H_2O_2$ rather than with an organic substrate. Second, and unexpectedly, $Fe^{III}$–OOH (**3**) reacts more rapidly with $H_2O_2$ in comparison to the rate that it undergoes O–O bond homolysis to form an $Fe^{IV}$=O species in the first place.

Ligand exchange, i.e. $Fe^{III}$–OR to $Fe^{III}$–OOH (**3**), precedes the oxidation of both organic substrates (eq 2) and $H_2O_2$ (eq 3). In the present study we show that O–O bond homolysis is relatively slow and is not competitive with the oxidation of $H_2O_2$ to $O_2$ by **3**. The reaction bifurcation seen for $Fe^{III}$–OOH presents a dichotomy in that $H_2O_2$ must be present in order to form $Fe^{IV}$=O (**4**), but the steady-state concentration of $H_2O_2$ should be less than that of $Fe^{III}$–OOH (**3**), in order that O–O bond homolysis to form $Fe^{IV}$=O and a HO• radical can take place and hence oxidation of organic substrates to occur. Hence, efficiency with respect to oxidation of organic substrates is increased, as observed in the present study, by maintaining a low steady-state concentrations of $H_2O_2$.

In conclusion, we show that the oxidation of organic substrates by reactive iron species competes with the reaction of these same species with $H_2O_2$ and hence wasteful disproportionation of the terminal oxidant. A substantial increase in oxidant efficiency is achieved by maintaining a pseudo-steady-state concentration of $H_2O_2$ that is below that of the catalyst itself. Furthermore, far from only being a metastable intermediate on route to an $Fe^{IV}$=O species, the $Fe^{III}$–OOH complex is kinetically competent in its reaction with $H_2O_2$. The conclusions reached in the present study have implications with regard to our approach to oxidation catalysis with iron catalysts with pentadentate ligands and in a wider perspective hold implications for the mechanisms invoked for catalase type reactions in both biomimetic and bioinorganic systems.

## ASSOCIATED CONTENT

### Supporting Information

The Supporting Information is available free of charge on the ACS Publications website at DOI: 10.1021/acscatal.8b02326.

Details of physical and computational methods, additional spectroscopic data, and coordinates for calculated species (PDF)

## AUTHOR INFORMATION

### Corresponding Author

*E-mail for W.R.B.: w.r.browne@rug.nl.

### ORCID

Apparao Draksharapu: 0000-0001-7897-3230
Marcel Swart: 0000-0002-8174-8488
Wesley R. Browne: 0000-0001-5063-6961

### Present Address

#A.D.: Department of Chemistry and Center for Metals in Biocatalysis, 207 Pleasant St. SE, University of Minnesota, Minneapolis, Minnesota 55455, United States.

### Notes

The authors declare no competing financial interest.



DOI: 10.1021/acscatal.8b02326
ACS Catal. 2018, 8, 9665–9674

## ■ ACKNOWLEDGMENTS

The COST association action CM1305 ECOSTBio (STSM grant 34080), the European Research Council (ERC 279549, W.R.B.), the labex arcane (ANR-11-LABX-003), MINECO (CTQ2014-59212-P and CTQ2015-70851-ERC, M.S.), Gen-Cat (2014SGR1202, MS), FEDER (UNGI10-4E-801, M.S.), and the Chinese Scholarship Council (CSC) are acknowledged for financial support.

## ■ REFERENCES

(1) Costas, M.; Mehn, M. P.; Jensen, M. P.; Que, L. Dioxygen Activation at Mononuclear Nonheme Iron Active Sites: Enzymes, Models, and Intermediates. *Chem. Rev.* **2004**, *104* (2), 939−986.

(2) Ghosh, A.; Mitchell, D. A.; Chanda, A.; Ryabov, A. D.; Popescu, D. L.; Upham, E. C.; Collins, G. J.; Collins, T. J. Catalase−Peroxidase Activity of Iron(III)−TAML Activators of Hydrogen Peroxide. *J. Am. Chem. Soc.* **2008**, *130* (45), 15116−15126.

(3) Roelfes, G.; Lubben, M.; Hage, R.; Que, L., Jr.; Feringa, B. L. Catalytic Oxidation with a Non-Heme Iron Complex That Generates a Low-Spin $Fe^{III}$OOH Intermediate. *Chem. - Eur. J.* **2000**, *6* (12), 2152−2159.

(4) Kim, Y. M.; Cho, K.-B.; Cho, J.; Wang, B.; Li, C.; Shaik, S.; Nam, W. A Mononuclear Non-Heme High-Spin Iron(III)-Hydroperoxo Complex as an Active Oxidant in Sulfoxidation Reactions. *J. Am. Chem. Soc.* **2013**, *135* (24), 8838−8841.

(5) Geng, C.; Ye, S.; Neese, F. Analysis of Reaction Channels for Alkane Hydroxylation by Nonheme Iron(IV)-Oxo Complexes. *Angew. Chem., Int. Ed.* **2010**, *49* (33), 5717−5720.

(6) Park, J.; Lee, Y.-M.; Nam, W.; Fukuzumi, S. Brønsted Acid-Promoted C−H Bond Cleavage via Electron Transfer from Toluene Derivatives to a Protonated Nonheme Iron(IV)-Oxo Complex with No Kinetic Isotope Effect. *J. Am. Chem. Soc.* **2013**, *135* (13), 5052−5061.

(7) Rana, S.; Dey, A.; Maiti, D. Mechanistic Elucidation of C−H Oxidation by Electron Rich Non-Heme Iron(IV)−oxo at Room Temperature. *Chem. Commun.* **2015**, *51* (77), 14469−14472.

(8) Draksharapu, A.; Angelone, D.; Quesne, M. G.; Padamati, S. K.; Gómez, L.; Hage, R.; Costas, M.; Browne, W. R.; de Visser, S. P. Identification and Spectroscopic Characterization of Nonheme Iron(III) Hypochlorite Intermediates. *Angew. Chem., Int. Ed.* **2015**, *54* (14), 4357−4361.

(9) Park, J.; Morimoto, Y.; Lee, Y.-M.; Nam, W.; Fukuzumi, S. Unified View of Oxidative C−H Bond Cleavage and Sulfoxidation by a Nonheme Iron(IV)−Oxo Complex via Lewis Acid-Promoted Electron Transfer. *Inorg. Chem.* **2014**, *53* (7), 3618−3628.

(10) Rohde, J.-U.; In, J.-H.; Lim, M. H.; Brennessel, W. W.; Bukowski, M. R.; Stubna, A.; Münck, E.; Nam, W.; Que, L. Crystallographic and Spectroscopic Characterization of a Nonheme Fe(IV)═O Complex. *Science* **2003**, *299* (5609), 1037−1039.

(11) Nam, W.; Lee, Y.-M.; Fukuzumi, S. Tuning Reactivity and Mechanism in Oxidation Reactions by Mononuclear Nonheme Iron(IV)-Oxo Complexes. *Acc. Chem. Res.* **2014**, *47* (4), 1146−1154.

(12) Cho, K.; Wu, X.; Lee, Y.; Kwon, Y. H.; Shaik, S.; Nam, W. Evidence for an Alternative to the Oxygen Rebound Mechanism in C−H Bond Activation by Non-Heme Fe(IV)═O Complexes. *J. Am. Chem. Soc.* **2012**, *134* (50), 20222−20225.

(13) Kumar, D.; Hirao, H.; Que, L.; Shaik, S. Theoretical Investigation of C−H Hydroxylation by $(N4Py)Fe^{IV}O^{2+}$: An Oxidant More Powerful than P450? *J. Am. Chem. Soc.* **2005**, *127* (22), 8026−8027.

(14) Kaizer, J.; Klinker, E. J.; Oh, N. Y.; Rohde, J. U.; Song, W. J.; Stubna, A.; Kim, J.; Münck, E.; Nam, W.; Que, L. Nonheme $Fe^{IV}O$ Complexes That Can Oxidize the C-H Bonds of Cyclohexane at Room Temperature. *J. Am. Chem. Soc.* **2004**, *126* (2), 472−473.

(15) Sheldon, R. A.; Arends, I. W. C. E.; ten Brink, G.-J.; Dijksman, A. Green, Catalytic Oxidations of Alcohols. *Acc. Chem. Res.* **2002**, *35* (9), 774−781.

(16) Roelfes, G.; Lubben, M.; Hage, R.; Que, L., Jr.; Feringa, B. L. Catalytic Oxidation with a Non-Heme Iron Complex That Generates a Low-Spin FeIIIOOH Intermediate. *Chem. - Eur. J.* **2000**, *6* (12), 2152.

(17) Franke, A.; Van Eldik, R. Spectroscopic and Kinetic Evidence for the Crucial Role of Compound 0 in the P450cam-Catalyzed Hydroxylation of Camphor by Hydrogen Peroxide. *Chem. - Eur. J.* **2015**, *21* (43), 15201−15210.

(18) Solomon, E. I.; Wong, S. D.; Liu, L. V.; Decker, A.; Chow, M. S. Peroxo and Oxo Intermediates in Mononuclear Nonheme Iron Enzymes and Related Active Sites. *Curr. Opin. Chem. Biol.* **2009**, *13* (1), 99−113.

(19) Lehnert, N.; Neese, F.; Ho, R. Y. N.; Que, L.; Solomon, E. I. Electronic Structure and Reactivity of Low-Spin Fe(III)-Hydroperoxo Complexes: Comparison to Activated Bleomycin. *J. Am. Chem. Soc.* **2002**, *124* (36), 10810−10822.

(20) Sam, J. W.; Tang, X.-J.; Peisach, J. Electrospray Mass Spectrometry of Iron Bleomycin: Demonstration That Activated Bleomycin Is a Ferric Peroxide Complex. *J. Am. Chem. Soc.* **1994**, *116* (12), 5250−5256.

(21) Roelfes, G.; Lubben, M.; Chen, K.; Ho, R. Y. N.; Meetsma, A.; Genseberger, S.; Hermant, R. M.; Hage, R.; Mandai, S. K.; Young, V. G., Jr.; Zang, Y.; Kooijman, H.; Spek, A. L.; Que, L., Jr.; Feringa, B. L. Iron Chemistry of a Pentadentate Ligand That Generates a Metastable $Fe^{III}$-OOH Intermediate. *Inorg. Chem.* **1999**, *38* (8), 1929−1936.

(22) Liu, L. V.; Hong, S.; Cho, J.; Nam, W.; Solomon, E. I. Comparison of High-Spin and Low-Spin Nonheme FeIII−OOH Complexes in O−O Bond Homolysis and H-Atom Abstraction Reactivities. *J. Am. Chem. Soc.* **2013**, *135* (8), 3286−3299.

(23) Decker, A.; Chow, M. S.; Kemsley, J. N.; Lehnert, N.; Solomon, E. I. Direct Hydrogen-Atom Abstraction by Activated Bleomycin: An Experimental and Computational Study. *J. Am. Chem. Soc.* **2006**, *128* (14), 4719−4733.

(24) Faponle, A. S.; Quesne, M. G.; Sastri, C. V.; Banse, F.; de Visser, S. P. Differences and Comparisons of the Properties and Reactivities of Iron(III)−hydroperoxo Complexes with Saturated Coordination Sphere. *Chem. - Eur. J.* **2015**, *21* (3), 1221−1236.

(25) Hirao, H.; Li, F.; Que, L., Jr.; Morokuma, K. Theoretical Study of the Mechanism of Oxoiron(IV) Formation from $H_2O_2$ and a Nonheme Iron(II) Complex: O-O Cleavage Involving Proton-Coupled Electron Transfer. *Inorg. Chem.* **2011**, *50* (14), 6637−6648.

(26) Li, F.; Van, H. K. M.; Meier, K. K.; Munck, E.; Que, L. $Sc^{3+}$-Triggered Oxoiron(IV) Formation from $O_2$ and Its Non-Heme Iron(II) Precursor via a $Sc^{3+}$−Peroxo−$Fe^{3+}$ Intermediate. *J. Am. Chem. Soc.* **2013**, *135* (28), 10198−10201.

(27) Li, F.; Meier, K. K.; Cranswick, M. A.; Chakrabarti, M.; Van Heuvelen, K. M.; Munck, E.; Que, L. Characterization of a High-Spin Non-Heme Fe(III)-OOH Intermediate and Its Quantitative Conversion to an Fe(IV)═O Complex. *J. Am. Chem. Soc.* **2011**, *133* (19), 7256−7259.

(28) Brown-Marshall, C. D.; Diebold, A. R.; Solomon, E. I. Reaction Coordinate of Isopenicillin N Synthase: Oxidase versus Oxygenase Activity. *Biochemistry* **2010**, *49* (6), 1176−1182.

(29) Quiñonero, D.; Morokuma, K.; Musaev, D. G.; Mas-Ballesté, R.; Que, L. Metal-Peroxo versus Metal-Oxo Oxidants in Non-Heme Iron-Catalyzed Olefin Oxidations: Computational and Experimental Studies on the Effect of Water. *J. Am. Chem. Soc.* **2005**, *127* (18), 6548−6549.

(30) Braymer, J. J.; O'Neill, K. P.; Rohde, J. U.; Lim, M. H. The Reaction of a High-Valent Nonheme Oxoiron(IV) Intermediate with Hydrogen Peroxide. *Angew. Chem., Int. Ed.* **2012**, *51* (22), 5376−5380.

(31) Lubben, M.; Meetsma, A.; Wilkinson, E. C.; Feringa, B.; Que, L. Nonheme Iron Centers in Oxygen Activation: Characterization of an Iron(III) Hydroperoxide Intermediate. *Angew. Chem., Int. Ed. Engl.* **1995**, *34* (13−14), 1512−1514.

(32) Draksharapu, A.; Li, Q.; Logtenberg, H.; van den Berg, T. A.; Meetsma, A.; Killeen, J. S.; Feringa, B. L.; Hage, R.; Roelfes, G.;



DOI: 10.1021/acscatal.8b02326
*ACS Catal.* 2018, 8, 9665−9674

Browne, W. R. Ligand Exchange and Spin State Equilibria of $Fe^{II}$(N4Py) and Related Complexes in Aqueous Media. *Inorg. Chem.* **2012**, *51* (2), 900−913.
(33) Chen, J.; Draksharapu, A.; Harvey, E.; Rasheed, W.; Que, L.; Browne, W. R. Direct Photochemical Activation of Non-Heme Fe(IV)═O Complexes. *Chem. Commun.* **2017**, *53* (91), 12357−12360.
(34) McCreery, R. L. *Raman Spectroscopy for Chemical Analysis*; Wiley: 2005; Vol. *225*.
(35) Baerends, E. J.; Autschbach, J.; Berces, A.; Bo, C.; Boerrigter, P. M.; Cavallo, L.; Chong, D. P.; Deng, L.; Dickson, R. M.; Ellis, D. E.; Fan, L.; Fischer, T. H.; Fonseca Guerra, C.; van Gisbergen, S. J. A.; Groeneveld, J. A.; Gritsenko, O. V.; Grüning, M.; Harris, F. E.; van den Hoek, P.; Jacobsen, H.; van Kessel, G.; Kootstra, F.; van Lenthe, E.; Osinga, V. P.; Patchkovskii, S.; Philipsen, P. H. T.; Post, D.; Pye, C. C.; Ravenek, W.; Ros, P.; Schipper, P. R. T.; Schreckenbach, G.; Snijders, J. G.; Solà, M.; Swart, M.; Swerhone, D.; te Velde, G.; Vernooijs, P.; Versluis, L.; Visser, O.; van Wezenbeek, E.; Wiesenekker, G.; Wolff, S. K.; Woo, T. K.; Ziegler, T. *ADF 20016.01*; SCM: Amsterdam, 20016.
(36) te Velde, G.; Bickelhaupt, F. M.; Baerends, E. J.; Fonseca Guerra, C.; van Gisbergen, S. J. A.; Snijders, J. G.; Ziegler, T. Chemistry with ADF. *J. Comput. Chem.* **2001**, *22* (9), 931−967.
(37) Swart, M.; Bickelhaupt, F. M. QUILD: QUantum-Regions Interconnected by Local Descriptions. *J. Comput. Chem.* **2008**, *29* (5), 724−734.
(38) Padamati, S. K.; Angelone, D.; Draksharapu, A.; Primi, G.; Martin, D. J.; Tromp, M.; Swart, M.; Browne, W. R. Transient Formation and Reactivity of a High-Valent Nickel(IV) Oxido Complex. *J. Am. Chem. Soc.* **2017**, *139* (25), 8718−8724.
(39) Becke, A. D. Density-Functional Exchange-Energy Approximation with Correct Asymptotic Behavior. *Phys. Rev. A: At., Mol., Opt. Phys.* **1988**, *38* (6), 3098−3100.
(40) Perdew, J. P. Density-Functional Approximation for the Correlation Energy of the Inhomogeneous Electron Gas. *Phys. Rev. B: Condens. Matter Mater. Phys.* **1986**, *33* (12), 8822−8824.
(41) Grimme, S.; Antony, J.; Ehrlich, S.; Krieg, H. A Consistent and Accurate Ab Initio Parametrization of Density Functional Dispersion Correction (DFT-D) for the 94 Elements H-Pu. *J. Chem. Phys.* **2010**, *132* (15), 154104.
(42) Swart, M. A. New Family of Hybrid Density Functionals. *Chem. Phys. Lett.* **2013**, *580* (0), 166−171.
(43) Swart, M.; Gruden, M. Spinning around in Transition-Metal Chemistry. *Acc. Chem. Res.* **2016**, *49* (12), 2690−2697.
(44) Swart, M.; Rösler, E.; Bickelhaupt, F. M. Proton Affinities in Water of Maingroup-Element Hydrides − Effects of Hydration and Methyl Substitution. *Eur. J. Inorg. Chem.* **2007**, *2007* (23), 3646−3654.
(45) McDonald, A. R.; Que, L. High-Valent Nonheme Iron-Oxo Complexes: Synthesis, Structure, and Spectroscopy. *Coord. Chem. Rev.* **2013**, *257*, 414−428.
(46) Draksharapu, A.; Li, Q.; Roelfes, G.; Browne, W. R. Photo-Induced Oxidation of [$Fe^{II}$(N4Py)$CH_3CN$] and Related Complexes. *Dalt. Trans.* **2012**, *41* (42), 13180−13190.
(47) Park, M. J.; Lee, J.; Suh, Y.; Kim, J.; Nam, W. Reactivities of Mononuclear Non-Heme Iron Intermediates Including Evidence That Iron(III)-Hydroperoxo Species Is a Sluggish Oxidant. *J. Am. Chem. Soc.* **2006**, *128*, 2630−2634.



DOI: 10.1021/acscatal.8b02326
*ACS Catal.* 2018, 8, 9665−9674